REPORT

Structure of RNA 3′-phosphate cyclase bound to substrate RNA

KEVIN K. DESAI,[1] CRAIG A. BINGMAN,[1] CHIN L. CHENG,[1] GEORGE N. PHILLIPS JR.,[1,2] and RONALD T. RAINES[1,3]

[1]Department of Biochemistry, University of Wisconsin–Madison, Madison, Wisconsin 53706, USA
[2]BioSciences at Rice and Department of Chemistry, Rice University, Houston, Texas 77005, USA
[3]Department of Chemistry, University of Wisconsin–Madison, Madison, Wisconsin 53706, USA

ABSTRACT

RNA 3′-phosphate cyclase (RtcA) catalyzes the ATP-dependent cyclization of a 3′-phosphate to form a 2′,3′-cyclic phosphate at RNA termini. Cyclization proceeds through RtcA–AMP and RNA(3′)pp(5′)A covalent intermediates, which are analogous to intermediates formed during catalysis by the tRNA ligase RtcB. Here we present a crystal structure of *Pyrococcus horikoshii* RtcA in complex with a 3′-phosphate terminated RNA and adenosine in the AMP-binding pocket. Our data reveal that RtcA recognizes substrate RNA by ensuring that the terminal 3′-phosphate makes a large contribution to RNA binding. Furthermore, the RNA 3′-phosphate is poised for in-line attack on the P–N bond that links the phosphorous atom of AMP to N^{ε} of His307. Thus, we provide the first insights into RNA 3′-phosphate termini recognition and the mechanism of 3′-phosphate activation by an Rtc enzyme.

Keywords: RtcA; RNA 3′-phosphate termini; 2′,3′-cyclic phosphate termini

INTRODUCTION

RNA 2′,3′-cyclic phosphate termini play a significant role in RNA metabolism as intermediates in the chemical- or enzyme-catalyzed hydrolysis of the RNA phosphodiester backbone (Markham and Smith 1952; Brown and Todd 1953; Raines 1998), as intermediates in tRNA splicing and repair (Konarska et al. 1982; Filipowicz et al. 1983; Greer et al. 1983; Amitsur et al. 1987; Zillmann et al. 1991; Abelson et al. 1998; Nandakumar et al. 2008; Englert et al. 2011; Popow et al. 2011; Tanaka and Shuman 2011), and as recognition elements present on U6 snRNA (Lund and Dahlberg 1992). RNA 2′,3′-cyclic phosphate termini can be synthesized from 3′-phosphate (3′-p) termini in an ATP-dependent reaction catalyzed by RNA 3′-phosphate cyclase (RtcA), an enzyme conserved in bacteria, archaea, and eukarya (Filipowicz et al. 1983, 1985; Reinberg et al. 1985; Billy et al. 1999; Tanaka and Shuman 2009; Tanaka et al. 2010). The cyclization of RNA 3′-p termini proceeds through three nucleotidyl transfer steps (Fig. 1A). In the first step, RtcA reacts with ATP and a divalent metal ion to form a covalent RtcA–AMP intermediate and release PP_i; in the second step, the AMP moiety is transferred to the RNA 3′-p terminus to form an RNA(3′)pp(5′)A intermediate; and in the third step, the vicinal 2′-OH attacks the activated 3′-p to form a 2′,3′-cyclic phosphate and release AMP (Filipowicz et al. 1985; Billy et al. 1999; Tanaka et al. 2010).

RtcA and the tRNA ligase RtcB are the only known enzymes that activate RNA 3′-p termini (Filipowicz et al. 1985; Chakravarty et al. 2012), with each enzyme proceeding through two analogous reaction steps to catalyze RNA 3′-p activation (Fig. 1A; Supplemental Fig. S1). Despite no structural similarities between RtcA and RtcB, both enzymes proceed through enzyme-(histidine-N^{ε})–NMP and RNA(3′)pp(5′)N intermediates (Filipowicz et al. 1985; Billy et al. 1999; Tanaka et al. 2010; Chakravarty et al. 2012; Desai et al. 2013). In the case of cyclization, the activated RNA 3′-p then undergoes nucleophilic attack by the vicinal 2′-OH, whereas RtcB catalyzes the attack of a 5′-OH terminus to form a 3′,5′-phosphodiester linkage. The genes encoding RtcA and RtcB are localized into an operon in *Escherichia coli* and other bacterial taxa. The mechanism of nucleotidylation of histidine residues in RtcA and RtcB has been elucidated (Tanaka et al. 2010; Chakravarty et al. 2011; Englert et al. 2012; Desai et al. 2013); however, the location of the RNA binding sites and the mechanism of RNA 3′-p nucleotidylation remain unknown for each enzyme. Moreover, how RtcA and RtcB avoid

Corresponding author: rtraines@wisc.edu
Article published online ahead of print. Article and publication date are at http://www.rnajournal.org/cgi/doi/10.1261/rna.045823.114.

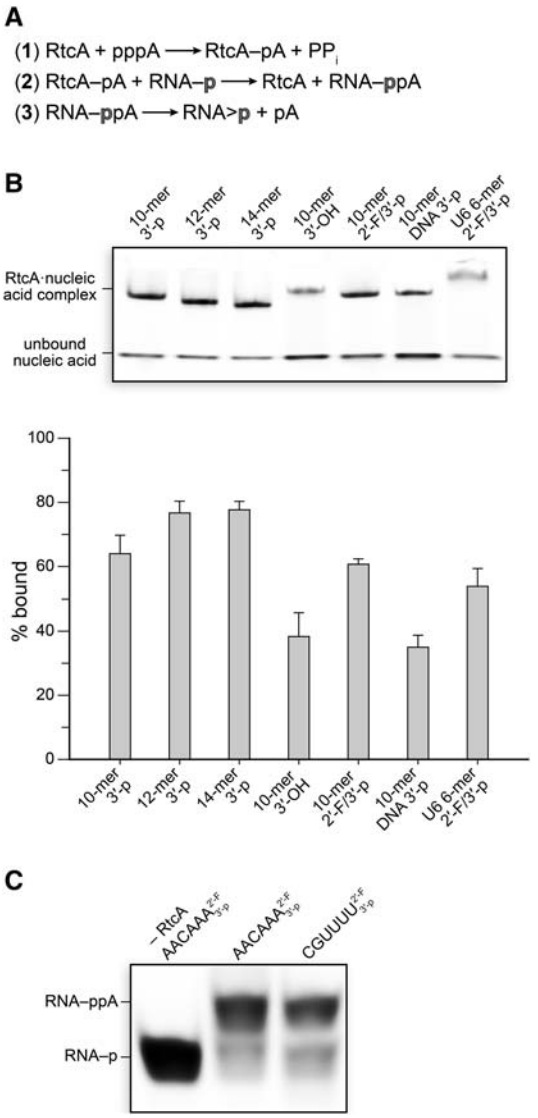

FIGURE 1. The three-step mechanism of RNA 3′-p termini cyclization and of RtcA RNA binding and RNA 3′-p activation assays. (*A*) The cyclization of RNA 3′-p termini to form 2′,3′-cyclic phosphate termini occurs in three nucleotidyl transfer steps, which are (1) RtcA histidine nucleotidylation, (2) RNA 3′-p nucleotidylation, and (3) cyclization via attack from the vicinal 2′-OH. (*B*) Gel-shift assays demonstrating nucleic acid binding to RtcA. Native RtcA (1 μM) was mixed with the specified RNA (1 μM) in 25 μL solutions of 50 mM HEPES–NaOH buffer (pH 7.5), containing NaCl (200 mM). The sequences of the 10-, 12-, and 14-mer were FAM–5′-AAAUAACAAA-3′-p, FAM–5′-AAAAAUAACAAA-3′-p, and FAM–5′-AAAAAAAUAACAAA-3′-p, respectively. The sequence of the U6 6-mer was FAM–5′-CGUUUU-3′-p. RNA binding was analyzed by native PAGE followed by band quantification using densitometry. Reported values are the mean ± SE for three separate experiments. (*C*) RNA 3′-p activation assays. Activation assays were performed in 25 μL solutions of 50 mM Tris–HCl buffer (pH 7.4), containing NaCl (0.3 M), ATP (0.1 mM), $MgCl_2$ (1 mM), RtcA (1 μM), and the indicated FAM-labeled RNA (1 μM). Reaction mixtures were incubated for 10 min at 75°C, and an equal volume of RNA gel-loading buffer (5× TBE containing 7 M urea, 20% v/v glycerol, and 15 mg/mL blue dextran) was added before urea–PAGE analysis. Reported values are the mean ± SE for three separate experiments.

binding to the abundant RNA 3′-OH termini *in cellulo* has remained an important unanswered question.

We sought to understand the molecular determinants for RNA 3′-p termini recognition and the mechanism of its activation by solving a crystal structure of RtcA in complex with substrate RNA. Previously, we have had success obtaining crystal structures of the tRNA ligase RtcB, as well as its activator Archease, from the hyperthermophilic archaeon *Pyrococcus horikoshii* (Desai et al. 2013, 2014). Thus, we reasoned that RtcA from *P. horikoshii* could likewise be suitable for crystallographic studies. The high evolutionary conservation of RtcA suggests that studies on the archaeal enzyme would be broadly applicable. Here we report X-ray crystal structures of RtcA that reveal (1) significant conformational changes accompanying RNA binding, (2) the exquisite RNA 3′-p termini recognition strategy evolved by RtcA, and (3) the mechanism of RNA 3′-p activation.

RESULTS AND DISCUSSION

RtcA RNA binding and RNA 3′-p activation assays

First, we interrogated the RNA binding and catalytic properties of *P. horikoshii* RtcA. Gel-shift assays demonstrated that RtcA binds short 3′-p terminated RNAs (Fig. 1B). Remarkably, when RtcA was mixed 1:1 with the 12- or 14-mer 3′-p terminated RNA, ~80% of the RNA remained bound to RtcA upon native-PAGE analysis. A 3′-OH terminated RNA and a 3′-p terminated DNA had reduced RtcA binding affinities. Likewise, human RtcA has been shown to discriminate strictly against 3′-OH RNA termini binding and to display an absolute requirement for 3′-p termini (Tanaka and Shuman 2009). The RNA 3′-OH termini binding that we observe with *P. horikoshii* RtcA likely stems from the rigidity of the hyperthermophilic enzyme at room temperature (Wolf-Watz et al. 2004), a characteristic that facilities the crystallization of thermophilic proteins. Additionally, an RNA consisting of the terminal 6 nucleotides (nt) of yeast U6 snRNA was able to bind, demonstrating a lack of nucleobase specificity in the RtcA active site (Fig. 1B).

To investigate the catalytic activity of RtcA, we developed an RNA 3′-p activation assay that uses a substrate RNA with a 3′-p/2′-F terminus. The 2′-F substituent maintains a ribose ring pucker similar to that observed with a 2′-OH; however, the 2′-F disallows the final cyclization step. Hence, our RtcA assay detects formation of the activated RNA intermediate. We favor this assay over traditional assays that detect 2′,3′-cyclic phosphate termini formation because the final cyclization step is RtcA independent (Filipowicz and Vicente 1990) and because the greater difference in the electrophoretic mobility between RNA–p and RNA–ppA facilitates analysis. Activation assays demonstrated that *P. horikoshii* RtcA is an active catalyst when the essential cofactors ATP and Mg(II) are supplied (Fig. 1C). We found that the activity assays work better with shorter RNAs and

observed RtcA activity with 6-nt RNA substrates having two different sequences.

Crystal structure of an RtcA·RNA complex

We pursued a crystal structure of RtcA in complex with the 12-mer 3′-p-terminated RNA. We solved the crystal structure of an RtcA·RNA complex to a resolution of 2.0 Å. Omit electron density maps indicated the presence of adenosine (which copurified with RtcA) in the AMP-binding pocket and of a 3′-p terminated RNA only 5 nt in length bound to each RtcA protomer (Fig. 2A; Table 1; Supplemental Fig. S2). RtcA·RNA crystal formation took 4 wk, and it is likely that a contaminating ribonuclease trimmed off 7 nt from the 5′ end of the RNA prior to crystallization. Superposition of our apoRtcA (refined to a resolution of 1.9 Å) and RtcA·RNA structures reveals high overall similarity (RMSD of 1.1 Å between corresponding C^{α} atoms); however, significant conformational changes are localized to the RNA binding site (Fig. 2B). The maximal C^{α} displacement is 5.1 Å at Asn38, which is located on a loop formed by residues 37–42 that moves toward the bound RNA (Supplemental Fig. S3).

RtcA has three nucleotide-binding sites for the RNA 3′-p substrate, which are all occupied by adenines (A3, A4, and A5) (Fig. 2C). Indeed, a trinucleotide RNA has been shown to have the minimal length for an RtcA substrate (Genschik et al. 1997). Adenine 1 (A1) and cytosine 2 (C2), located on the RNA 5′ terminus extend beyond the RNA binding cleft and make interactions with a symmetry-related RtcA molecule. The nucleobases in all three binding sites are in the *anti* conformation, and the ribose ring pucker is 2′-*endo* for A3 and A5 but 3′-*endo* for A4. The A3 nucleobase makes van der Waals contact with Pro158, while the backbone amides of Ala92 and Pro158 form hydrogen bonds with the ribose 2′-OH (Fig. 2D). The A3 5′ phosphoryl group forms a hydrogen bond with Tyr157, while the 3′ phosphoryl group

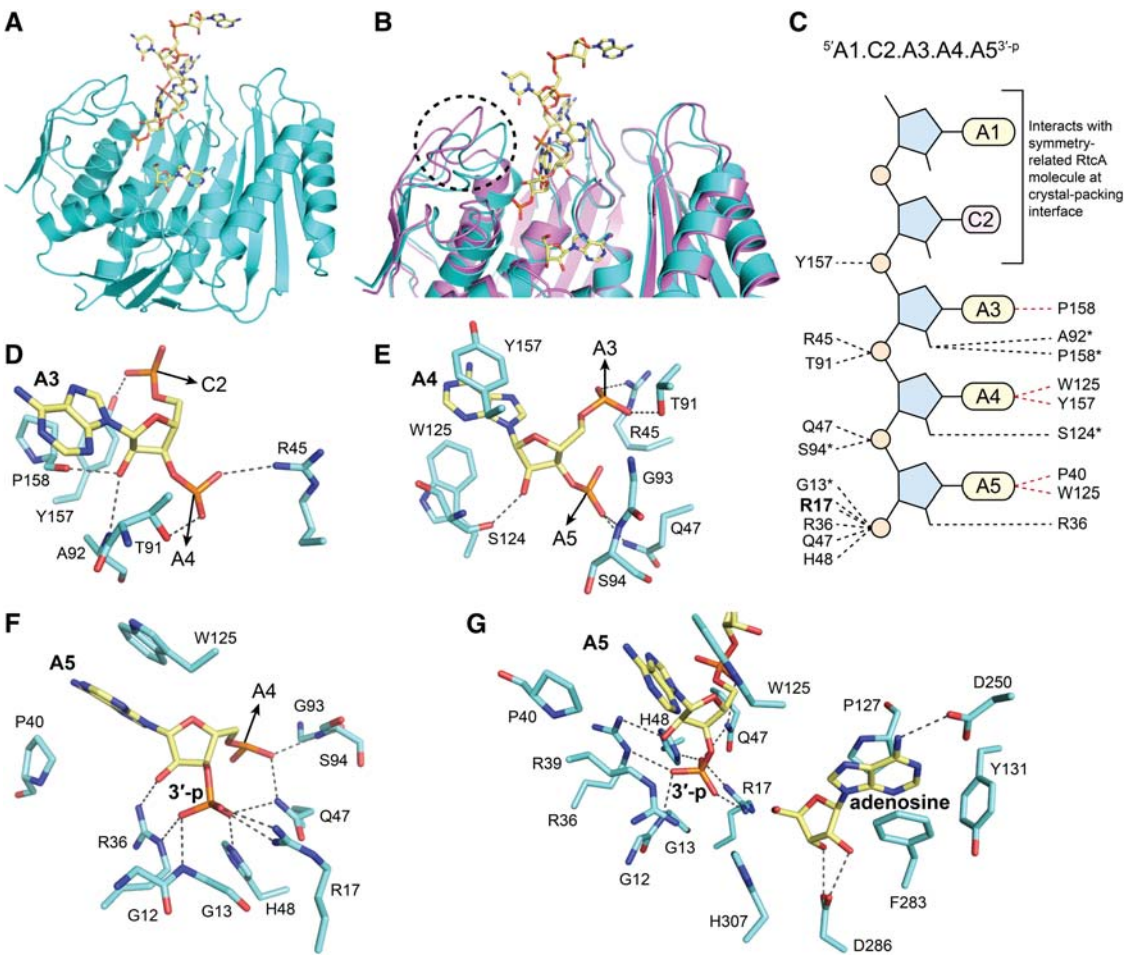

FIGURE 2. Crystal structures of *P. horikoshii* RtcA. (*A*) Structure of RtcA (cartoon representation) with bound RNA and adenosine (depicted as sticks). (*B*) Superposition of apoRtcA (magenta) and RtcA·RNA (teal). The dashed black circle highlights the RtcA region that undergoes the largest conformational change upon RNA binding. (*C*) Schematic depicting RtcA hydrogen bonding (dashed black lines) and van der Waals interactions (dashed magenta lines) with the bound RNA. Asterisks denote backbone interactions. (*D*) The A3 nucleotide-binding site. (*E*) The A4 nucleotide-binding site. (*F*) The A5 nucleotide-binding and RNA 3′-p binding sites. (*G*) The active site, illustrating the RNA 3′-p poised for in-line attack on the P–N bond of an RtcA–(His307-N^{ε})–AMP intermediate. Adenosine occupies the AMP-binding pocket.

TABLE 1. Crystallographic data collection and refinement statistics

	apoRtcA	RtcA·RNA
Data collection		
Space group	$P3_221$	$P2_12_12_1$
Cell dimensions *a*, *b*, *c* (Å)	89.9, 89.9, 146.89	83.92, 110.26, 127.65
Radiation source	23-ID-B APS	23-ID-D APS
Wavelength	0.91165 Å	0.97934 Å
Resolution (Å)	44.95–1.9 (1.97–1.9)	46.14–2.04 (2.11–2.04)
Total reflections	311864	561799
R_{sym} or R_{merge}	0.067 (0.961)	0.115 (1.380)
R_{pim}	0.028 (0.455)	0.050 (0.476)
Mean $I/\sigma I$	17.16 (2.03)	13.55 (1.47)
Completeness (%)	98.85 (96.23)	99.6 (54.55)
Redundancy	5.9 (4.6)	7.4 (7.4)
CC1/2	0.914 (0.572)	0.932 (0.729)
CC*	0.974 (0.853)	0.982 (0.918)
Refinement		
Resolution (Å)	44.95–1.9 (1.97–1.9)	46.14 –2.04 (2.11–2.04)
Unique reflections	53,389 (2453)	71,784 (4089)
R_{work}/R_{free}	0.179/0.231 (0.262/0.317)	0.155/0.197 (0.207/0.263)
B-factors (Å^2)		
Protein	30.3	46.0
Solvent	37.4	58.6
Ramachandran plot	97% favored	97% favored
RMSDs		
Bond lengths (Å)	0.008	0.012
Bond angles (°)	1.12	1.55
Protomers	2	2
Protein residues	682	682
Nonprotein molecules	546 waters Two citrates	610 waters One HEPES Two adenosines 10 RNA nucleotides
PDB ID	4o89	4o8j

Values in parentheses are for the highest-resolution shell. The real-space correlation coefficients for the 10 RNA nucleotides have a range of 0.97–1.

forms hydrogen bonds with Arg45 and Thr91. The A4 nucleobase is sandwiched between Trp125 and Tyr157 (Fig. 2E). The backbone oxygen of Ser124 forms a hydrogen bond with the A4 ribose 2′-OH, while the 3′ phosphoryl group forms hydrogen bonds with Gln47 and the backbone nitrogen of Ser94. The A5 nucleobase makes van der Waals contact with Pro40 and Trp125 (Fig. 2F). The A5 ribose 2′-OH forms a hydrogen bond with Arg36. Hydrogen bonding with the ribose 2′-OH in all three nucleotide-binding sites enforces a strong preference for RNA over DNA. The notable absence of polar contacts between RtcA and the nucleobases enables promiscuity in RNA sequence specificity.

RtcA discriminates against 3′-OH termini by allocating a large proportion of the RNA binding interactions to the 3′-p terminus. Remarkably, 40% of all hydrogen bonds formed with the RNA substrate are with the three nonbridging oxygen atoms of the terminal 3′-p (Fig. 2C). A network of six hydrogen bonds engages the terminal 3′-p in the RtcA active site. Arg17 donates two hydrogen bonds to the 3′-p, while Arg36, Gln47, His48, and the backbone nitrogen of Gly13 also form hydrogen bonds with the terminal 3′-p (Fig. 2F). The five residues that interact with the terminal 3′-p display strict evolutionary conservation (Supplemental Fig. S4).

Mechanism of AMP transfer to an RNA 3′-p

Occupancy of the AMP-binding pocket by adenosine in our RtcA·RNA structure enables the simultaneous observation of both RtcA substrates within the active site (Fig. 2G). The adenosine ribose adopts a 2′-*endo* pucker, and Asp286 accepts hydrogen bonds from the 2′-OH and 3′-OH groups. The adenosine nucleobase is in the *anti* conformation and makes van der Waals contact with Pro127 and Phe283. The adenine exocyclic amino group donates a hydrogen bond to Asp250, distinguishing the archaeal RtcA from the *E. coli* enzyme, which makes no polar contacts with the adenine nucleobase (Tanaka et al. 2010).

The transfer of phosphoryl groups to and from enzymic histidine residues is known to proceed by in-line attack (Wang et al. 2006; Rigden 2008). In catalysis by RtcA, the RNA 3′-p activation step is likely to proceed by in-line attack of a 3′-p oxygen atom on the P–N bond that links the phosphorous atom of AMP to a nitrogen atom of a histidine residue. Indeed, the RNA 3′-p in our structure is poised appropriately for in-line attack on a P–N bond to N^{ε} of His307 (Fig. 2G, Supplemental Fig. S5). The enzyme-catalyzed transfer of phosphophodiesters is known to proceed through an associative mechanism having a pentavalent transition state in which negative charge accumulates on the two nonbridging oxygen atoms (Knowles 1980; Cleland and Hengge 2006; Lassila et al. 2011). Based on our RtcA·RNA structure, the RNA 3′-p activation step is likely promoted by Arg39, which is in a position to stabilize incipient negative charge. In the active site of the RNA ligase RtcB, NMP transfer from histidine to the RNA 3′-p is likely promoted by a Mn(II) ion, which coordinates a nonbridging phosphate oxygen of histidine–GMP (Desai et al. 2013). Likewise, classical ATP-dependent RNA and DNA ligases transfer AMP by in-line attack of a 5′-p on a lysine–AMP intermediate. In Chlorella virus DNA ligase, for example, 5′-p activation is likely promoted by two lysine residues, which

coordinate a nonbridging phosphate oxygen of lysine–AMP (Nair et al. 2007).

Structure-guided mutagenesis of RtcA

Substitution of RtcA residues that interact with the substrate RNA revealed their importance for both RNA binding and RNA 3′-p activation. Substitution of Arg17, which donates two hydrogen bonds to the terminal 3′-p, had the largest effect on RNA binding (Fig. 3A). RtcA variants with substitutions of Arg17, Arg36, Arg39, and His307 were inactive in RNA 3′-p activation assays (Fig. 3B). The inactivity of these variants is likely due to impairment in RtcA–AMP formation, which has been demonstrated for corresponding variants of human RtcA (Tanaka and Shuman 2009).

The exquisite RNA termini recognition strategy evolved by RtcA could be common to RtcB and possibly other unknown enzymes that recognize nucleic acid 3′-p termini (Tanaka et al. 2011; Desai and Raines 2012). The RtcB active site is unique from that of RtcA with respect to its two metal-binding sites, which could help to coordinate and/or stabilize the 3′-p and activated 3′-p intermediate (Englert et al. 2012; Desai et al. 2013). RtcB has the difficult task of preventing intramolecular cyclization of the activated RNA intermediate (Chakravarty et al. 2012), whereas RtcA has evolved to release this intermediate into solution (Filipowicz and Vicente 1990). The allocation of a large proportion of hydrogen-bonding interactions to the RNA 3′-p terminus by RtcA enables discrimination against 3′-OH termini binding due to a lack of favorable interactions.

The precise molecular recognition of substrates is a hallmark of highly evolved enzymes (Jensen 1976). A molecular recognition predicament analogous to the one faced by RtcA is exemplified by enzymes dependent on the redox cofactors NAD(H) or NADP(H) for activity. The two cofactors differ only by a single phosphoryl group, and redox enzymes generally have a strong preference for either NAD(H) or NADP(H). Typically, a preference for NADP(H) is enforced by an arginine residue that forms a hydrogen bond with the dichotomous adenosine 2′-p (Carugo and Argos 1997). Here we have provided the first insights into the molecular recognition of RNA with a terminal 3′-p, an essential component of substrates for the enzyme RtcA.

MATERIALS AND METHODS

RtcA production and purification

The *P. horikoshii rtcA* gene was synthesized on gBlocks (Integrated DNA Technologies) using codons optimized for expression in *E. coli*. The *rtcA* gene was assembled into pQE70-*lacI* via Gibson assembly. Native RtcA was expressed in BL21 cells by growing in Terrific Broth medium at 37°C to an OD_{600} of 0.6, inducing with IPTG (0.5 mM) and continuing growth for 3 h. Cells were harvested by centrifugation and resuspended at 8 mL/g of wet pellet in buffer A (50 mM MES–NaOH at pH 5.6, containing 45 mM NaCl). Cells were lysed by passage through a cell disruptor (Constant Systems) at 20,000 psi, and the lysate was clarified by centrifugation at 20,000*g* for 1 h. Bacterial proteins were precipitated and removed by incubating the lysate for 25 min at 70°C followed by centrifugation at 20,000*g* for 20 min. The clarified lysate was then loaded onto

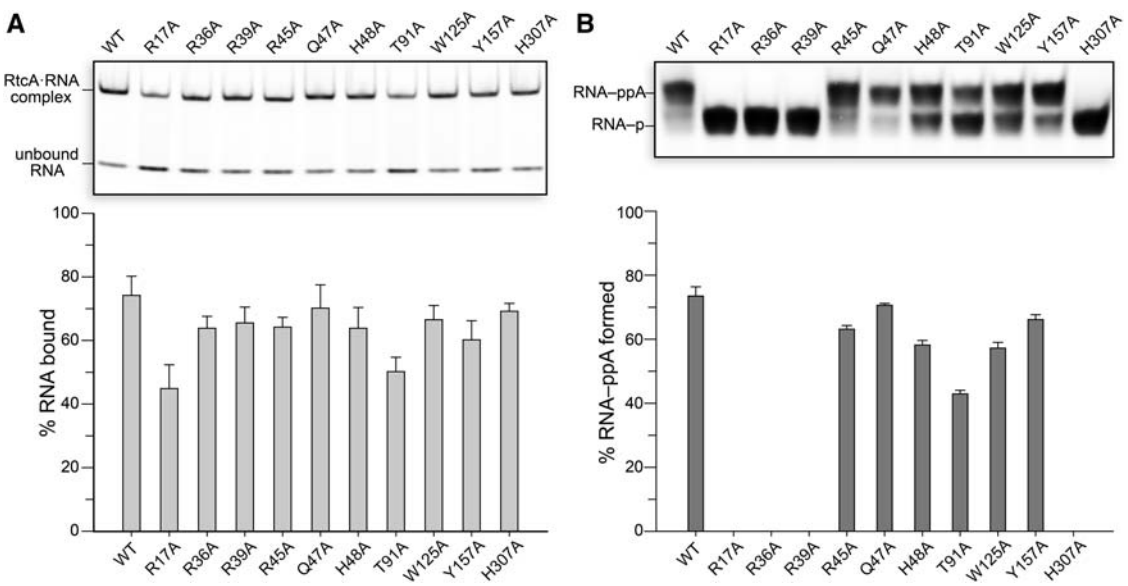

FIGURE 3. Structure-guided mutagenesis of RtcA. (*A*) RNA binding assays with RtcA variants. The RNA used for binding assays was FAM–5′-AAAUAACAAA-3′-p. RNA binding was analyzed by native PAGE followed by band quantification using densitometry. Reported values are the mean ± SE for three separate experiments. (*B*) RNA 3′-p activation assays with RtcA variants. The substrate RNA for activation assays was FAM–5′-AACAAA-3′-p/2′-F. Reaction products were resolved by urea–PAGE analysis. Reported values are the mean ± SE for three separate experiments.

a 5-mL column of HiTrap HP SP cation-exchange resin (GE Healthcare). The resin was washed with 50 mL of buffer A, and RtcA was eluted with a gradient of NaCl (45 mM–1.0 M) in buffer A over 20 column volumes. Fractions containing purified RtcA were dialyzed overnight at 4°C against 2 L of 10 mM HEPES–NaOH buffer (pH 7.5), containing NaCl (200 mM). The protein was flash-frozen in liquid nitrogen and stored at −80°C. The concentration of RtcA was calculated from the A_{280} value and a calculated (ExPASy) extinction coefficient of $\varepsilon_{280} = 34950\ M^{-1}cm^{-1}$.

RNA binding assays

Native RtcA (1 µM) was mixed with the specified RNA (1 µM) in 25 µL solutions of 50 mM HEPES–NaOH buffer (pH 7.5), containing NaCl (200 mM). The sequences of the 10-, 12-, and 14-mer were FAM–5′-AAAUAACAAA-3′-p, FAM–5′-AAAAAUAACAAA-3′-p, and FAM–5′-AAAAAAAUAACAAA-3′-p, respectively. The addition of $MgCl_2$ to the RNA binding assays did not affect RNA binding (data not shown). RNA binding to RtcA was instantaneous and did not require incubation. An equal volume of RNA native polyacrylamide gel electrophoresis gel-loading buffer (TBE containing 30% v/v glycerol and 0.01% w/v bromophenol blue) was added to the binding assays before analysis. RNA binding assays were resolved by native PAGE on an Any kD gel (Bio-Rad), and RNA was visualized by fluorescence scanning with a Typhoon FLA9000 imager (GE Healthcare). RNA binding was quantified with ImageQuant TL software (GE Healthcare). Reported values are the mean ± SE for three separate experiments.

RNA 3′-p activation assays

RNA 3′-p activation assays were performed in 25-µL solutions of 50 mM Tris–HCl buffer (pH 7.4), containing NaCl (0.3 M), ATP (0.1 mM), $MgCl_2$ (1 mM), RtcA (1 µM), and a specified RNA (1 µM). Reaction mixtures were incubated for 10 min at 75°C, and an equal volume of RNA gel-loading buffer (5× TBE containing 7 M urea, 20% v/v glycerol, and 15 mg/mL blue dextran) was added before analysis. Reaction products were separated on an 18% w/v urea–polyacrylamide gel, and RNA was visualized by fluorescence scanning with a Typhoon FLA9000 imager (GE Healthcare). Product was quantified with ImageQuant TL software (GE Healthcare). Reported values are the mean ± SE for three separate experiments.

RtcA crystallization, data collection, and structure determination

The apoRtcA sample was prepared by concentrating native RtcA to 12 mg/mL by ultrafiltration using a spin concentrator (Amicon 10,000 MWCO, Millipore). For preparation of the RtcA·RNA sample, the protein was first concentrated, and then the 12-mer 3′-p terminated RNA (5′-AAAAAUAACAAA-3′-p) was added in a 1.2-fold molar excess, which resulted in a final RtcA protein concentration of 20 mg/mL. The protein samples were flash-frozen in liquid nitrogen and stored at −80°C. The apoRtcA sample was first screened with the Index HT 96-well screen (Hampton Research) and the JCSG+ 96-well screen (Qiagen) using the sitting drop vapor diffusion method. The Mosquito robot (TTP Labtech) was used to pipette 150 nL of reservoir solution and 150 nL of apoRtcA sample into each well of the screens. Trays were incubated at 20°C, and crystals appeared within 1 wk in well H10 of the Index HT screen. The conditions from well H10 of Index HT were optimized using the hanging drop vapor diffusion method. Optimized apoRtcA crystals were grown by mixing 1 µL of protein solution with 1 µL of reservoir solution of 0.10 M trisodium citrate buffer (pH 7.0), containing polyethylene glycol 3,350 (20% w/v). Trays were incubated at 20°C, and crystals appeared within 1 wk. The apoRtcA crystals were harvested, cryoprotected in reservoir solution containing glycerol (20% v/v), and flash-frozen in liquid nitrogen. The RtcA·RNA sample was crystallized using the sitting drop vapor diffusion method. The RtcA·RNA sample was screened for crystallization using the Index HT 96-well screen. The Mosquito robot was used to pipette 150 nL of reservoir solution and 150 nL of RtcA·RNA sample into each well of the screen. Trays were incubated at 20°C, and crystals appeared after 4 wk. RtcA·RNA crystals appeared in condition F1 of the screen, which contained 0.10 M, HEPES–NaOH buffer (pH 7.5), polyethylene glycol 3,350 (10% w/v), and L-proline (0.2 M). RtcA·RNA crystals were harvested directly from well F1 of the 96-well screen, cryoprotected in reservoir solution containing glycerol (30% v/v), and flash-frozen in liquid nitrogen. X-ray diffraction data were collected at the General Medicine and Cancer Institutes Collaborative Access Team (GM/CA-CAT) at Argonne National Laboratory. Data sets were indexed and scaled using HKL2000 (Otwinowski and Minor 1997). Structures were solved by molecular replacement using *E. coli* RtcA as a starting model (PDB entry 3tut) (Chakravarty et al. 2011) followed by autosolve in Phenix (Adams et al. 2010). The RNA was built in with COOT (Emsley and Cowtan 2004), and the models were completed using alternating rounds of manual model building using COOT and refinement with phenix.refine. Structure quality was assessed with MolProbity (Davis et al. 2007), and figures were generated using PyMOL (DeLano 2002). Omit maps were calculated with Phenix.

DATA DEPOSITION

The coordinates and structure factors for apoRtcA and RtcA·RNA have been deposited in the Protein Data Bank under accession codes 4o89 and 4o8j, respectively.

SUPPLEMENTAL MATERIAL

Supplemental material is available for this article.

ACKNOWLEDGMENTS

We thank M. Becker and C. Ogata for GM/CA beamline assistance at the Advanced Photon Source and A.A. Hoskins for helpful discussion. Support came from National Institutes of Health (NIH) grants F32 GM100681 (to K.K.D.), U01 GM098248 (to G.N.P.), and R01 CA073808 (to R.T.R.). GM/CA-CAT has been funded by Y1-CO-1020 and Y1-GM-1104. The APS was supported by the US Department of Energy (DOE) under contract no. DE-AC02-06CH11357.

Received April 13, 2014; accepted July 22, 2014.

REFERENCES

Abelson J, Trotta CR, Li H. 1998. tRNA splicing. *J Biol Chem* **273:** 12685–12688.

Adams PD, Afonine PV, Bunkóczi G, Chen VB, Davis IW, Echols N, Headd JJ, Hung LW, Kapral GJ, Grosse-Kunstleve RW, et al. 2010. PHENIX: a comprehensive Python-based system for macromolecular structure solution. *Acta Crystallogr D Biol Crystallogr* **66:** 213–221.

Amitsur M, Levitz R, Kaufman G. 1987. Bacteriophage T4 anticodon nuclease, polynucleotide kinase, and RNA ligase reprocess the host lysine tRNA. *EMBO J* **6:** 2499–2503.

Billy E, Hess D, Hofsteenge J, Filipowicz W. 1999. Characterization of the adenylation site in the RNA 3′-terminal phosphate cyclase from *Escherichia coli*. *J Biol Chem* **274:** 34955–34960.

Brown DM, Todd AR. 1953. Nucleotides. Part XXI. The action of ribonuclease on simple esters of the monoribonucleotides. *J Chem Soc* **1953:** 2040–2049.

Carugo O, Argos P. 1997. NADP-dependent enzymes. I: conserved stereochemistry of cofactor binding. *Proteins* **28:** 10–28.

Chakravarty AK, Smith P, Shuman S. 2011. Structures of RNA 3′-phosphate cyclase bound to ATP reveal the mechanism of nucleotidyl transfer and metal-assisted catalysis. *Proc Natl Acad Sci* **108:** 21034–21039.

Chakravarty AK, Subbotin R, Chait BT, Shuman S. 2012. RNA ligase RtcB splices 3′-phosphate and 5′-OH ends via covalent RtcB-(histidinyl)-GMP and polynucleotide-(3′)pp(5′)G intermediates. *Proc Natl Acad Sci* **109:** 6072–6077.

Cleland WW, Hengge AC. 2006. Enzymatic mechanisms of phosphate and sulfate transfer. *Chem Rev* **106:** 3252–3278.

Davis IW, Leaver-Fay A, Chen VB, Block JN, Kapral GJ, Wang X, Murray LW, Arendall WB III, Snoeyink J, Richardson JS, et al. 2007. MolProbity: all-atom contacts and structure validation for proteins and nucleic acids. *Nucleic Acids Res* **35:** W375–W383.

DeLano WL. 2002. *The PyMOL molecular graphics system*. DeLano Scientific, San Carlos, CA.

Desai KK, Raines RT. 2012. tRNA ligase catalyzes the GTP-dependent ligation of RNA with 3′-phosphate and 5′-hydroxyl termini. *Biochemistry* **51:** 1333–1335.

Desai KK, Bingman CA, Phillips GN Jr, Raines RT. 2013. Structures of the noncanonical RNA ligase RtcB reveal the mechanism of histidine guanylylation. *Biochemistry* **52:** 2518–2525.

Desai KK, Cheng CL, Bingman CA, Phillips GN Jr, Raines RT. 2014. A tRNA splicing operon: Archease endows RtcB with dual GTP/ATP cofactor specificity and accelerates RNA ligation. *Nucleic Acids Res* **42:** 3931–3942.

Emsley P, Cowtan K. 2004. *Coot*: model-building tools for molecular graphics. *Acta Crystallogr D Biol Crystallogr* **60:** 2126–2132.

Englert M, Sheppard K, Aslanian A, Yates JR III, Söll D. 2011. Archaeal 3′-phosphate RNA splicing ligase characterization identifies the missing component in tRNA maturation. *Proc Natl Acad Sci* **108:** 1290–1295.

Englert M, Xia S, Okada C, Nakamura A, Tanavde V, Yao M, Eom SH, Konigsberg WH, Söll D, Wang J. 2012. Structural and mechanistic insights into guanylylation of RNA-splicing ligase RtcB joining RNA between 3′-terminal phosphate and 5′-OH. *Proc Natl Acad Sci* **109:** 15235–15240.

Filipowicz W, Vicente O. 1990. RNA 3′-terminal phosphate cyclase from HeLa cells. *Methods Enzymol* **181:** 499–510.

Filipowicz W, Konarska M, Gross HJ, Shatkin AJ. 1983. RNA 3′-terminal phosphate cyclase activity and RNA ligation in HeLa cell extract. *Nucleic Acids Res* **11:** 1405–1418.

Filipowicz W, Strugala K, Konarska M, Shatkin AJ. 1985. Cyclization of RNA 3′-terminal phosphate by cyclase from HeLa cells proceeds via formation of N(3′)pp(5′)A activated intermediate. *Proc Natl Acad Sci* **82:** 1316–1320.

Genschik P, Billy E, Swianiewicz M, Filipowicz W. 1997. The human RNA 3′-terminal phosphate cyclase is a member of a new family of proteins conserved in Eucarya, Bacteria and Archaea. *EMBO J* **16:** 2955–2967.

Greer CL, Peebles CL, Gegenheimer P, Abelson J. 1983. Mechanism of action of a yeast RNA ligase in tRNA splicing. *Cell* **32:** 537–546.

Jensen RA. 1976. Enzyme recruitment in evolution of new function. *Annu Rev Microbiol* **30:** 409–425.

Knowles JR. 1980. Enzyme-catalyzed phosphoryl transfer reactions. *Annu Rev Biochem* **49:** 877–919.

Konarska M, Filipowicz W, Gross HJ. 1982. RNA ligation via 2′-phosphomonoester, 3′,5′-phosphodiester linkage: requirement of 2′,3′-cyclic phosphate termini and involvement of a 5′-hydroxyl polynucleotide kinase. *Proc Natl Acad Sci* **79:** 1474–1478.

Lassila JK, Zalatan JG, Herschlag D. 2011. Biological phosphoryl-transfer reactions: understanding mechanism and catalysis. *Annu Rev Biochem* **80:** 669–702.

Lund E, Dahlberg JE. 1992. Cyclic 2′,3′-phosphates and nontemplated nucleotides at the 3′ end of spliceosomal U6 small nuclear RNA's. *Science* **255:** 327–330.

Markham R, Smith JD. 1952. The structure of ribonucleic acids. I. Cyclic nucleotides produced by ribonuclease and by alkaline hydrolysis. *Biochem J* **52:** 552–557.

Nair PA, Nandakumar J, Smith P, Odell M, Lima CD, Shuman S. 2007. Structural basis for nick recognition by a minimal pluripotent DNA ligase. *Nat Struct Mol Biol* **14:** 770–778.

Nandakumar J, Schwer B, Schaffrath R, Shuman S. 2008. RNA repair: an antidote to cytotoxic eukaryal RNA damage. *Mol Cell* **31:** 278–286.

Otwinowski Z, Minor W. 1997. Processing of X-ray diffraction data collected in oscillation mode. *Methods Enzymol* **276:** 307–326.

Popow J, Englert M, Weitzer S, Schleiffer A, Mierzwa B, Mechtler K, Trowitzsch S, Will CL, Lührmann R, Söll D, et al. 2011. HSPC117 is the essential subunit of a human tRNA splicing ligase complex. *Science* **331:** 760–764.

Raines RT. 1998. Ribonuclease A. *Chem Rev* **98:** 1045–1065.

Reinberg D, Arenas J, Hurwitz J. 1985. The enzymatic conversion of 3′-phosphate terminated RNA chains to 2′,3′-cyclic phosphate derivatives. *J Biol Chem* **260:** 6088–6097.

Rigden DJ. 2008. The histidine phosphatase superfamily: structure and function. *Biochem J* **409:** 333–348.

Tanaka N, Shuman S. 2009. Structure–activity relationships in human RNA 3′-phosphate cyclase. *RNA* **15:** 1865–1874.

Tanaka N, Shuman S. 2011. RtcB is the RNA ligase component of an *Escherichia coli* RNA repair operon. *J Biol Chem* **286:** 7727–7731.

Tanaka N, Smith P, Shuman S. 2010. Structure of the RNA 3′-phosphate cyclase-adenylate intermediate illuminates nucleotide specificity and covalent nucleotidyl transfer. *Structure* **18:** 449–457.

Tanaka N, Chakravarty AK, Maughan B, Shuman S. 2011. Novel mechanism of RNA repair by RtcB via sequential 2′,3′-cyclic phosphodiesterase and 3′-phosphate/5′-hydroxyl ligation reactions. *J Biol Chem* **286:** 43134–43143.

Wang Y, Liu L, Wei Z, Cheng Z, Lin Y, Gong W. 2006. Seeing the process of histidine phosphorylation in human bisphosphoglycerate mutase. *J Biol Chem* **281:** 39642–39648.

Wolf-Watz M, Thai V, Henzler-Wildman K, Hadjipavlou G, Eisenmesser EZ, Kern D. 2004. Linkage between dynamics and catalysis in a thermophilic-mesophilic enzyme pair. *Nat Struct Mol Biol* **11:** 945–949.

Zillmann M, Gorovsky MA, Phizicky EM. 1991. Conserved mechanism of tRNA splicing in eukaryotes. *Mol Cell Biol* **11:** 5410–5416.